Journal of Operation and Automation in Power Engineering

Vol. XX, No. XX, XXXX, Pages: XXXX (Proofed)

http://joape.uma.ac.ir

1978
University of Mohaghegh Ardabili

Research Paper

Enhancing Voltage Stability in Renewable-Integrated Indian Utility System: A Multi-Objective FACTS Placement Approach Using Analytic Hierarchy Process

Karuppasamy Anthony[1, *] and *Venkadesan Arunachalam*[2]

[1] *Department of Electrical and Electronics Engineering, Kangeyam Institute of Technology, Tiruppur, India.*
[2] *Department of Electrical and Electronics Engineering, National Institute of Technology Puducherry, Karaikal, India.*

Abstract— *Voltage stability remains a significant challenge in renewable-integrated power systems due to the intermittent and variable nature of solar and wind energy. This study presents a multi-objective optimization framework to enhance voltage stability by strategically placing Unified Power Flow Controllers (UPFCs). The approach prioritizes improving voltage profiles, increasing loadability margins, and minimizing power losses to ensure reliable system performance in hybrid renewable environments. The Analytic Hierarchy Process (AHP) systematically evaluates and ranks potential UPFC placements based on multiple decision criteria, effectively addressing integration challenges and system constraints. The methodology is validated using a modified Indian utility 62-bus system with high renewable energy penetration under diverse operating conditions. Results indicate a 17.24% improvement in voltage stability margin, a 17.72% reduction in active power loss, and a 6.53% decrease in reactive power loss compared to conventional placement methods. These findings confirm the effectiveness of the proposed approach in enhancing voltage stability, reducing losses, and improving overall system reliability. This work provides a robust decision-making tool for utilities and stakeholders aiming to optimize voltage stability in modern, renewable-rich power grids.*

Keywords—Renewable energy, voltage stability, flexible AC transmission systems, multi-criteria decision making, analytic hierarchy process, unified power flow controller.

NOMENCLATURE

Abbreviations

AHP	Analytic Hierarchy Process
ARAS	Additive Ratio Assessment
CPF	Continuation Power Flow
CR	Consistency Ratio
FACTS	Flexible AC Transmission Systems
MCDM	Multi-Criteria Decision Making
MOORA	Multi-Objective Optimization based on Ratio Analysis
PSAT	Power System Analysis Toolbox
RES	Renewable Energy Sources
SPV	Solar Photovoltaic
STATCOM	Static Synchronous Compensator
SVC	Static VAR Compensator
TCSC	Thyristor Controlled Series Compensator
TOPSIS	Technique for Order Preference by Similarity to Ideal Solution
UPFC	Unified Power Flow Controller
VIKOR	VIekriterijumsko KOmpromisno Rangiranje
VSM	Voltage Stability Margin
WF	Wind Farm

Symbols

λ	Load parameter
λ_{max}	Maximum / critical load parameter
$\omega_1, \omega_2, \omega_3$	Weighting factors for the objective functions
θ_i, θ_j	Sending-end and receiving-end phase angles
B_{ii}, B_{jj}, B_{ij}	Self and mutual susceptance of the line
f_1, f_2, f_3	Single objective functions
G_{ii}, G_{jj}, G_{ij}	Self and mutual conductance of the line
P_i, P_j	Sending-end and receiving-end real power
P_{cR}, Q_{cR}	Series converter active and reactive powers
P_{vR}, Q_{vR}	Shunt converter active and reactive powers
Q_i, Q_j	Sending-end and receiving-end reactive power
V_i, V_j	Voltage at sending-end and receiving-end buses
V_{cR}, δ_{cR}	Controllable magnitude and phase angle of series converter
V_{vR}, δ_{vR}	Controllable magnitude and phase angle of shunt converter

Received: 21 Jan. 2025
Revised: 25 Mar. 2025
Accepted: 08 Apr. 2025
*Corresponding author:
E-mail: samydeeebe@gmail.com (K. Anthony)
DOI: 10.22098/joape.2025.16598.2280

1. INTRODUCTION

Globally, approximately 660 million people are expected to lack access to electricity, highlighting a persistent challenge in achieving universal energy access. The United Nations has established seventeen Sustainable Development Goals (SDGs) to address such critical issues. This goal underscores the importance of expanding clean energy solutions to bridge the energy access gap while promoting environmental sustainability and social equity. Achieving SDG is pivotal to enabling global progress in health, education, and economic development [1]. The increasing integration of RES, such as solar and wind power, into electrical networks, has significantly altered the dynamics of the power grid [2].

Although renewable energy offers considerable ecological benefits and reduces dependence on fossil fuels, it also introduces grid stability and voltage management challenges. The impact of wind energy on the VSM power system is examined in [3]. A solar-powered integrated power system for VSM estimation is suggested by [4]. As RES are integrated into the grid and traditional generation patterns transform, the dynamics of power systems are undergoing significant changes, posing new challenges to voltage stability [5].

In the contemporary landscape of power systems, ensuring voltage stability is paramount for reliable and efficient operation. Maintaining voltage stability has become challenging with the growing complexity of power grids and the increasing electricity demand [6]. The grid operators optimize the grid's performance to enhance efficiency and economic advantages. This affords operators a minimal cushion for load variations at load buses. The system may malfunction for a duration ranging from several seconds to numerous minutes [7].

The development of FACTS devices for reliable power system performance has been made possible by advances in power electronics technology [8]. In the previous 20 years, several power-electronic controllers have been developed. Voltage control is a significant application for FACTS controllers, and they are also incorporated into the electrical grid to minimize losses, control load flow, harmonic mitigation, and improve transient stability [9]. Compared to other FACTS controllers, the UPFC is preferred for voltage stability enhancement due to its unique and versatile capabilities, which offer comprehensive control over multiple power system parameters, fast dynamic response, and the ability to provide active and reactive power support [10]. This makes it far superior to other FACTS controllers when voltage stability is critical in a power system.

Recently, multi-objective methods have gained popularity for the best distribution of FACTS controllers [11]. Generally, learning and intelligent optimization algorithms determine the FACTS devices' optimal placement and capacity. Heuristic methods that provide the closest response are usually utilized instead of the mathematical model that delivers the most exact result [12]. However, selecting the most suitable locations involves various factors and criteria, making it a complex problem [13]. Different optimization techniques have been explored, including particle swarm optimization [14], genetic algorithms [15], and differential evolution [16]. While these methods offer valuable insights, they often require significant computational resources and do not always account for the multi-objective nature of the problem. Optimization methods become complex, and convergence takes longer to solve multi-objective problems. Hence, MCDM approaches have gained popularity in solving multi-objective problems more quickly.

In MCDM techniques, weights are numerical values assigned to each criterion to reflect its relative importance in decision-making. They help decision-makers prioritize specific criteria over others, depending on their objectives or preferences. The weights assigned to the criterion were deemed equivalent in a few of these articles [17, 18]. The decision maker's weighted criteria were applied in a few more articles [19, 20]. In certain papers, weights were applied equally, at decision-maker-determined values, and in various combinations based on various scenarios [21, 22]. In each experiment, the decision-makers assigned weights to the criteria based on the priority levels. Still, they had no control over the consistency of the authors [23] on scientific principles. Consequently, the reliability of the results displays a significant defect. The principal objective of this research is to close this gap in the literature.

The AHP emerges as a robust and widely adopted MCDM technique for decision-making in complex systems [24]. AHP provides a structured framework for systematically analyzing decision problems with multiple criteria and alternatives, facilitating informed and rational decision-making [25]. AHP provides a systematic way of handling multiple conflicting objectives, allowing for a balanced trade-off between performance metrics such as voltage stability, power loss reduction, and reactive power management.

The optimal placement of UPFC is a complex multi-objective problem influenced by network topology, load variations, and economic constraints. Various optimization techniques, including heuristic methods like PSO and GA, have been explored to determine the best UPFC placement. However, these methods often suffer from convergence issues and computational inefficiencies, particularly in large-scale networks. Additionally, existing research lacks a standardized approach to weighting criteria in MCDM techniques, leading to inconsistencies in placement strategies. Moreover, many studies assume deterministic load conditions, failing to account for the uncertainties in RES generation. Recent advancements in artificial intelligence, such as reinforcement learning and deep learning, offer promising solutions for real-time optimization. This study aims to bridge these gaps by developing a robust multi-objective optimization framework that enhances voltage stability while considering real-world constraints and renewable energy uncertainties. In light of those mentioned above, the best location for UPFC as a limited multi-objective optimization issue is discussed in this article. The MCDM-AHP technique achieves this goal by reducing the multi-objective optimization problem to a single objective function. In this paper, the three objectives, namely the maximizing loading margin range, minimizing the bus voltage deviation, and minimizing power losses, are considered simultaneously to identify the optimal location of UPFC.

The overarching goals of this research are:

- To design and implement efficient strategies to optimize power system operations, addressing the specific challenges of integrating renewable and sustainable energy sources at system and component levels.
- To optimize power flow while concurrently improving voltage stability, minimizing power losses, reducing voltage deviations, and enhancing the reliability of power supply in systems with significant renewable energy penetration.
- To analyze and model real-world renewable-integrated power systems, providing practical and scalable solutions to enhance operational efficiency and long-term reliability.

This study presents a novel approach for voltage stability enhancement in renewable-integrated power systems by strategically placing UPFCs using the AHP. Unlike previous studies focusing on IEEE test systems, this research is conducted on a practical Indian 62-bus utility system, making the findings more applicable to real-world scenarios. The proposed method evaluates the impact of varying solar, wind, and hybrid renewable energy penetration levels on voltage stability and identifies critical penetration limits. Unlike conventional heuristic-based methods, AHP provides a structured decision-making framework based on voltage deviation, real power loss, and load margin to determine optimal UPFC placement.

The approach's effectiveness is validated by comparing AHP with other MCDM techniques, including TOPSIS, MOORA, ARAS, VIKOR, and Mod-TOPSIS. Furthermore, the voltage stability margin is assessed using the CPF method, offering a dynamic evaluation under different loading conditions. These contributions make the study distinct and relevant to modern power systems with high renewable energy integration.

This study presents a multi-objective optimization framework to enhance voltage stability in renewable-integrated power systems by strategically placing UPFCs. The key contributions are:

- Introduced a structured decision-making process using the AHP to optimize UPFC placement, ensuring a balance between voltage stability, loadability margins, and power loss minimization.

- Conducted the study on a modified Indian utility 62-bus system with high renewable energy penetration, making the results more applicable to real-world power grids compared to IEEE test systems.
- Accounted for the intermittency of solar and wind power, addressing key challenges in hybrid renewable energy systems and ensuring grid stability under diverse operating scenarios.
- Validated the effectiveness of AHP by comparing it with other MCDM techniques, including TOPSIS, MOORA, ARAS, VIKOR, and Mod-TOPSIS, ensuring a robust decision-making approach.

Integrating MCDM techniques provides a robust decision-support tool for utilities and grid operators to optimize voltage stability in modern renewable-rich power systems.

2. Voltage Stability Analysis of Solar and Wind Integrated Power Systems

RESs, including wind and solar, are intrinsically fluctuant and intermittent, generating electricity contingent upon environmental factors, including solar radiation and wind velocity, which fluctuate quickly [26]. This inconsistency can cause swings in power production that, if not managed appropriately, may threaten the system's voltage stability. Precisely assessing the loading margin while integrating RES into the electrical system is crucial for maintaining grid stability and reliability. The positioning among these RES is essential for improving the loading margin.

VSM is crucial for power system dependability and serves as the reserve of voltage capacity exceeding the minimum allowable thresholds. It denotes a system's capacity to endure variations in generation and demand while preserving a stable voltage profile. The power system's loading margin is shown in Fig. 1. as the interval between the baseline loading point λ_o and the maximum permissible loading point λ_{max}. The load margin keeps on varying, as shown in Fig. 1, due to the intermittency nature of RES variations.

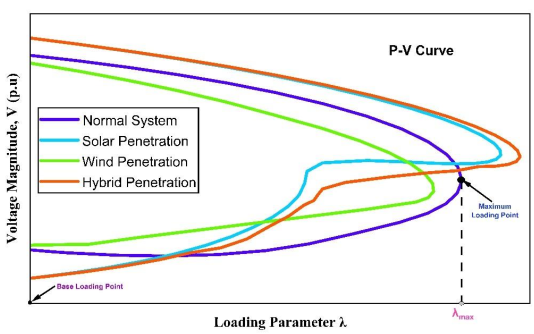

Fig. 1. Load margin variations in renewable integrated system.

The point at which the voltage begins to collapse is called the "nose point" of the P-V curve. Ensuring a power grid's reliable and secure operation relies heavily on the relationship between the loading margin and the power system stability level. The difference between the system's stability limit and the existing operational load is known as the loading margin. Increased stability results from a larger buffer against disruptions, which is indicated by a higher loading margin. In contrast, a smaller loading margin indicates that the system is operating near its stability limit, which increases its vulnerability to disturbances and instability. To study the impact of RES on voltage stability, solar and wind modeling is essential, which are briefed below,

2.1. Solar PV model

Several parts make up a solar photovoltaic system. These include a control system, a DC/AC converter, a photovoltaic array, and a maximum power point tracking system [27]. Two models in PSAT can be used to show solar photovoltaic devices.

- Constant P and Constant V control
- Constant P and Constant Q control

The constant P and constant V control modes are most useful for power system stability research, according to work by [27] that compares these two models in power system stability. In this work, solar photovoltaic power generation is thus represented by continuous P and constant V control models. Fig. 2. displays the block diagram for the converter model and the Constant P and V control methods.

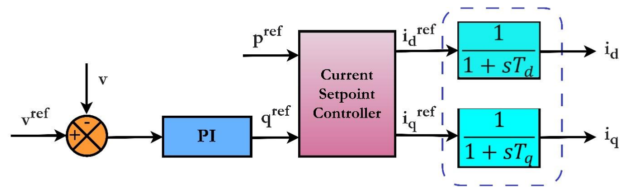

Fig. 2. A control strategy for a constant PV solar photovoltaic generator converter model.

The following equations define the model:

$$\begin{aligned} 0 &= v_0^{ref} - v^{ref} \\ \dot{x}_v &= K_i(v^{ref} - v) \\ 0 &= x_v + K_p(v^{ref} - v) - q^{ref} \end{aligned} \tag{1}$$

Equations for the model's definition in Eq. (1) and the shown in Fig. 2 p^{ref} is set point active power v_0^{ref} is the reference voltage, $T_d\&T_q$ is inverter time constants of d-axis and q-axis, K_p represents the voltage controller's proportional gain and K_i represents the voltage controller integral gain.

2.2. Wind turbine model

The wind is represented by the Weibull distribution utilized in PSAT [28]; this model is frequently employed in several wind modeling applications and has been applied in several prior research studies. The Weibull distribution is articulated as follows:

$$f(v_w, c, k) = \frac{k}{c^k} v_w^{(k-1)} e(-\frac{v_w}{c})^k \tag{2}$$

In this context, v_w represents the wind speed, while c and k are constants specified in the wind model data matrix.

The output power of a wind turbine is articulated as:

$$P_m = C_p(\lambda, \beta)\frac{1}{2} \cdot \rho \cdot A \cdot v^3 \tag{3}$$

Where, P_m denotes the mechanical output power, which is contingent upon air density (ρ), wind velocity (v), and blade characteristics C_p possesses the non-linear connection between (λ, β).

The predominant wind turbine models are the Squirrel Cage Induction Generator (SCIG) and the Doubly Fed Induction Generator (DFIG). Prior investigations have assessed the appropriateness of several models in power system stability. DFIG wind turbines provide superior performance in terms of power system stability. This study employed the DFIG wind turbine to generate wind electricity. The parameters for the DFIG model are sourced from Ref. [27].

In DFIG, the stator and rotor flux dynamics are far more rapid than the grids. Furthermore, the machine's converter control decouples the DFIG from the grid. Consequently, it can be articulated,

$$\begin{aligned}
&v_{ds} = \\
&-r_s i_{ds} + (x_s + x_\mu)\, i_{qs} + x_\mu i_{qr} \\
&v_{qs} = \\
&-r_s i_{qs} - ((x_s + x_\mu)\, i_{ds} + x_\mu i_{dr}) \\
&v_{dr} = \\
&-r_r i_{dr} + (1-\omega_m)\,((x_s + x_\mu)\, i_{qr} + x_\mu i_{qs}) \\
&v_{qr} = \\
&-r_r i_{dr} - (1-\omega_m)\,((x_s + x_\mu)\, i_{qr} + x_\mu i_{ds})
\end{aligned} \tag{4}$$

Here v_{ds}, $v_{qs}\&i_{ds}$, i_{qs} are stator voltages and currents on the d and q axes. v_{dr}, $v_{qr}\&i_{dr}$, i_{qr} are rotor voltages and currents on the d and q axes. r_s, r_r are resistances of the stator and rotor, x_s, x_r are self-reactance of the stator and rotor. x_μ represents the mutual reactance, then ω is the speed of the rotor.

Assuming no losses, the rotor's active power (P) can be regarded as the active power observed by the converter. Concerning reactive power (Q), the provided power to the grid can be determined by abandoning stator resistance and presuming that the d-axis aligns with the peak stator flux. Hence, the powers provided to the grid result in,

$$\begin{aligned}
&P = v_{ds} i_{ds} + v_{qs} i_{qs} + \\
&v_{dr} i_{dr} + v_{qr} i_{qr} \\
&Q = -\tfrac{x_\mu v i_{dr}}{x_s + x_\mu} - \tfrac{v^2}{x_\mu}
\end{aligned} \tag{5}$$

Rotor current limitations are determined as follows: v set to 1 per unit.

$$\begin{aligned}
&i_{qr}^{max} \approx -\tfrac{x_s + x_\mu}{x_\mu} P^{min} \\
&i_{qr}^{max} \approx -\tfrac{x_s + x_\mu}{x_\mu} P^{min} \\
&i_{qr}^{max} \approx -\tfrac{x_s + x_\mu}{x_\mu} Q^{min} - \tfrac{x_s + x_\mu}{x_\mu^2} \\
&i_{dr}^{max} \approx -\tfrac{x_s + x_\mu}{x_\mu} Q^{min} - \tfrac{x_s + x_\mu}{x_\mu^2}
\end{aligned} \tag{6}$$

3. Voltage Stability Enhancement using the UPFC Model

The voltage stability margin is generally enhanced by employing FACT devices. The UPFC was chosen because it provides good performance, which has been proven in the literature [29]. It can individually regulate three power system parameters: reactive power, line active power, and bus voltage. All three factors are controlled by the UPFC either concurrently or in any combination, provided no operating limitations are exceeded. To prevent thermal limitations from being exceeded and to boost the stability margin, UPFC control can alter line flow [30]. Fig. 3 depicts a straightforward schematic illustration of the UPFC and its corresponding equivalent circuit [31].

Three voltage sources comprise Fig. 3-(b), which depicts the UPFC equivalent circuit. Three voltage sources: one connected in series, the other in shunt, and the two are coupled using an active power constraint equation. The AC system is coupled to the two voltage sources by inductive reactance, which supports the VSC transformers. The UPFC voltage sources are,

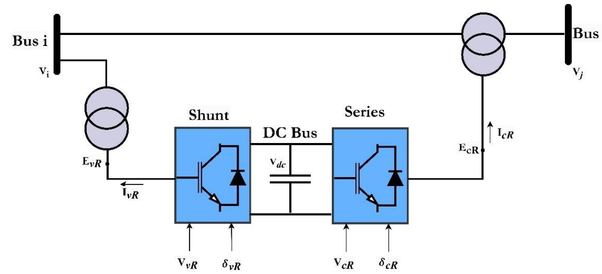

Fig. 3. a. The UPFC schematic diagram.

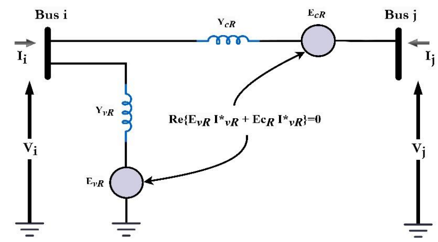

Fig. 3.b. The UPFC equivalent circuit.

Fig. 3. UPFC configuration: (a) schematic diagram and (b) equivalent circuit.

$$E_{vR} = V_{vR}\,(\cos\delta_{vR} + j\sin\delta_{vR}) \tag{7}$$

$$E_{cR} = V_{cR}\,(\cos\delta_{cR} + j\sin\delta_{cR}) \tag{8}$$

Where: V_{vR} and δ_{vR} are the voltage source's configurable phase angle and magnitude that correspond to the shunt converter, respectively:

$$V_{vR\,\min} \leq V_{vR} \leq V_{vR\,\max} \tag{9}$$

$$0 \leq \delta_{vR} \leq 2\pi \tag{10}$$

Where: V_{cR} and δ_{cR} are the voltage source's configurable phase angle and magnitude that serve as a representation of the series converter., respectively:

$$V_{cR\,\min} \leq V_{cR} \leq V_{cR\,\max} \tag{11}$$

$$0 \leq \delta_{cR} \leq 2\pi \tag{12}$$

The following are the equations for the reactive and active power at buses i and j:

$$\begin{aligned}
&P_i = \\
&V_i^2 G_{ii} + V_i V_j \Big[G_{ij}\cos(\theta_i - \theta_j) + B_{ij}\sin(\theta_i - \theta_j)\Big] \\
&+ V_i V_{cR}\Big[G_{ij}\cos(\theta_i - \delta_{cR}) + B_{ij}\sin(\theta_i - \delta_{cR})\Big] \\
&+ V_i V_{vR}\Big[G_{vR}\cos(\theta_i - \delta_{vR}) + B_{vR}\sin(\theta_i - \delta_{vR})\Big]
\end{aligned} \tag{13}$$

$$Q_i = -V_i^2 G_{ii} + V_i V_j \Big[G_{ij}\cos(\theta_i-\theta_j) - B_{ij}\sin(\theta_i-\theta_j)\Big] + V_i V_{cR}\Big[G_{ij}\cos(\theta_i-\delta_{cR}) - B_{ij}\sin(\theta_i-\delta_{cR})\Big] + V_i V_{vR}\Big[G_{vR}\cos(\theta_i-\delta_{vR}) - B_{vR}\sin(\theta_i-\delta_{vR})\Big] \tag{14}$$

$$P_j = V_j^2 G_{jj} + V_j V_i \Big[G_{ji}\cos(\theta_j-\theta_i) + B_{ji}\sin(\theta_j-\theta_i)\Big] + V_j V_{cR}\Big[G_{jj}\cos(\theta_j-\delta_{cR}) + B_{jj}\sin(\theta_j-\delta_{cR})\Big] \tag{15}$$

$$Q_j = -V_j^2 B_{jj} + V_j V_i \Big[G_{ji}\cos(\theta_j-\theta_i) - B_{ji}\sin(\theta_j-\theta_i)\Big] + V_j V_{cR}\Big[G_{jj}\cos(\theta_j-\delta_{cR}) - B_{jj}\sin(\theta_j-\delta_{cR})\Big] \tag{16}$$

The series converter's reactive and active powers are as follows:

$$P_{cR} = V_{cR}^2 G_{jj} + V_{cR} V_i [G_{ji}\cos(\delta_{cR}-\theta_i) + B_{ji}\sin(\delta_{cR}-\theta_i)] + V_j V_{cR}[G_{jj}\cos(\delta_{cR}-\theta_j) + B_{jj}\sin(\delta_{cR}-\theta_j)] \tag{17}$$

$$Q_{cR} = -V_{cR}^2 B_{jj} + V_{cR} V_i [G_{ji}\cos(\delta_{cR}-\theta_i) - B_{ji}\sin(\delta_{cR}-\theta_i)] + V_j V_{cR}[G_{jj}\cos(\delta_{cR}-\theta_j) - B_{jj}\sin(\delta_{cR}-\theta_j)] \tag{18}$$

The shunt converter's reactive and active powers are as follows:

$$P_{vR} = -V_{vR}^2 G_{vR} + V_{vR} V_i [G_{vR}\cos(\delta_{vR}-\theta_i) + B_{vi}\sin(\delta_{vR}-\theta_i)] \tag{19}$$

$$Q_{vR} = V_{vR}^2 B_{vR} + V_{vR} V_i [G_{vR}\sin(\delta_{vR}-\theta_i) - B_{vi}\cos(\delta_{vR}-\theta_i)] \tag{20}$$

4. AHP Approach for Finding the Optimal Location of UPFC

AHP helps in selecting the best location based on multiple criteria that impact the performance of the power system. The primary goal is to identify the optimal bus or line in the power grid to place the UPFC for maximum system stability and efficiency. Decision-making involves multiple criteria: loadability margin, bus voltage deviation, and active power losses. The concept of the AHP approach and the optimal location of UPFC using AHP are presented in this section.

4.1. Analytic hierarchy process

AHP is one of the MCDM techniques proposed by T.L. Saaty in the 1970s to compare options for criteria weights pairwise. This method evaluates several facts concurrently and methodically to identify each piece's relative value and meaning in the hierarchy. The numerical numbers found in the computations represent the weights or priority [32]. The initial stage in this technique is to build a hierarchical model. Pair-wise comparison matrices are created in the second phase to illustrate the relative significance of each variable [33].

The decision maker should assess each alternative in a decision analysis based on the pre-established criteria. The N options and NO criteria indicate the number of distinct load buses and the study's objectives, respectively. The global aim (first level), personal goals at the second level, and alternatives at the third level are the minimum levels at which a hierarchy is constructed in the AHP method [34]. Fig. 4 hierarchically presents the AHP solution structure. Specifying the objective and pair-comparison matrices following the first level's determination of the global objective is necessary.

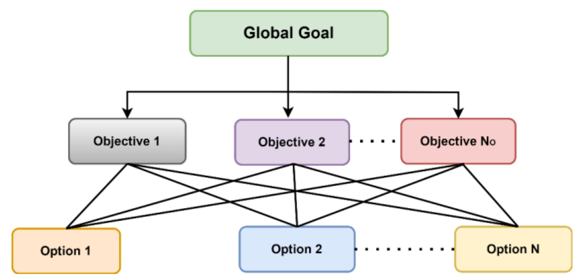

Fig. 4. Structure of the AHP method.

To illustrate each variable's relative importance for every level in a hierarchical structure, matrices are constructed with expert guidance. Values range from 1 to 9, with intervals of 2 expressing the following: extremely important, very important, strongly significant, somewhat important, and equally important. The nearby medians are 2, 4, 6, and 8 when five levels are inadequate [35]. After that, a pairwise comparison matrix is created by contrasting options under Table 1 [36].

Table 1. The Satay's Scale for relative judgments for the AHP method.

Scaling of importance	Interpretation	Clarification
1	Equal Important	Two options are equally beneficial to the objective.
3	Moderate Important	One objective is favored over another based on judgment and experience.
5	Strong Important	Experience and judgment greatly favor one objective over another.
7	Very Strong Important	One objective is much favored over the other, manifested in practice.
9	Extreme Important	The data that favors one conduct over another has the highest level of affirmation.
2, 4, 6, 8	In-between level	Intermediate level of importance.

Following the computation of pairwise comparisons, the constancy of the decisions is verified. The decision matrix can be approved if this number falls below a predetermined precision value. In other circumstances, the decision matrix is not consistent. Decisions must be modified and altered in these situations to produce a consistent matrix [37].

Nevertheless, absolute compatibility utilizing the amplitude-limited, discrete Saaty's scales cannot be verified by comparing the alternatives. To do this, values under the CR determined by matrix size may be processed using the AHP method. The CR value can be found as follows:

$$CR^{(j)} = \frac{CI^{(j)}}{RI} \tag{21}$$

The greatest eigenvalue λ_{max} is used to calculate the consistency index $CI^{(j)}$ in the following way:

$$CI^{(j)} = \frac{\lambda_{\max} - 1}{N - 1} \tag{22}$$

Table 2 displays the reference consistency index (RI), whose value is derived from the number of characteristics (N). When $CI^{(j)}$ is less than 0.1, the matrix $D^{(j)}$ is considered consistent. The index $CI^{(j)}$ is compared with RI.

4.2. Analytic hierarchy process for the optimal location of UPFC

A multi-objective optimization issue typically calls for simultaneously optimizing several objectives connected to inequality and equality constraints. The most significant load change that the power system in a bus or group of buses can sustain at the reference operating point is known as the VSM or load margin maximization, and it is achieved by using the widely used voltage collapse proximity index to improve voltage stability. Finding the smallest value of the sum of the objective functions is the aim of the task. Consequently, the inverse of maximum loadability can be used to represent the maximization of VSM:

$$f_1 = \frac{1}{\lambda_{\text{critical}}} \tag{23}$$

To enhance the voltage profile of the system and avoid voltage collapse, the FACTS controllers ought to be installed at the best locations. Consequently, it has been determined that the second goal is to minimize the bus voltage deviation. The objective function can be written as follows:

$$f_2 = \sum_{m=1}^{N} \left| V_m^{\text{ref}} - V_m \right| \tag{24}$$

The voltage at bus m is denoted by V_m, the number of buses is N, and the nominal voltage is represented by V_{mref}. This study considers a bus voltage range of 0.90–1.10 p.u. appropriate.

Reducing active power losses (P_{loss}) is also important from a budgetary standpoint. The following is a representation of P_{loss}:

$$f_3 = P_{\text{loss}} = \sum_{m=1}^{N} g_m \left[V_i^2 + V_j^2 - 2V_iV_j \cos(\delta_i - \delta_j) \right] \tag{25}$$

In this case, g_m represents the transmission line conductance, V_i denotes bus i voltage, V_j denotes bus j voltage, δ_i denotes bus i voltage angle, and δ_j denotes bus j voltage angle.

The hierarchal model is created by placing the goal, i.e., UPFC placement, at the top, and the criteria loadability margin, bus voltage deviation, and active power losses are in the second level, followed by the alternatives (potential UPFC locations) in the last level. Fig. 5 displays the flow diagram of an AHP implementation for the optimal location of UPFC.

The process starts with an objective definition and assessment criteria definition followed by the hierarchical model construction.

AHP converts subjective preferences like the importance of voltage stability into numerical values, making the decision process more objective. Eq. (26) can be used to define the objective function by considering the constraints on equality and inequality.

$$\text{Minimize } F = [f_1, f_2, f_3] \tag{26}$$

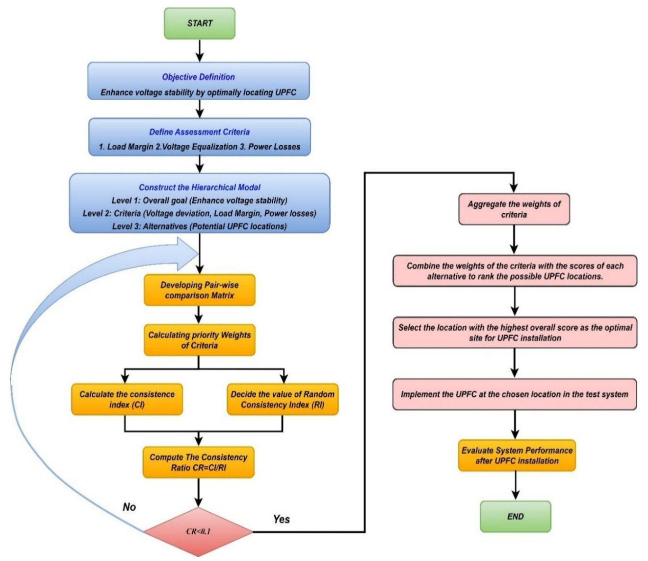

Fig. 5. AHP implementation flowchart for UPFC location.

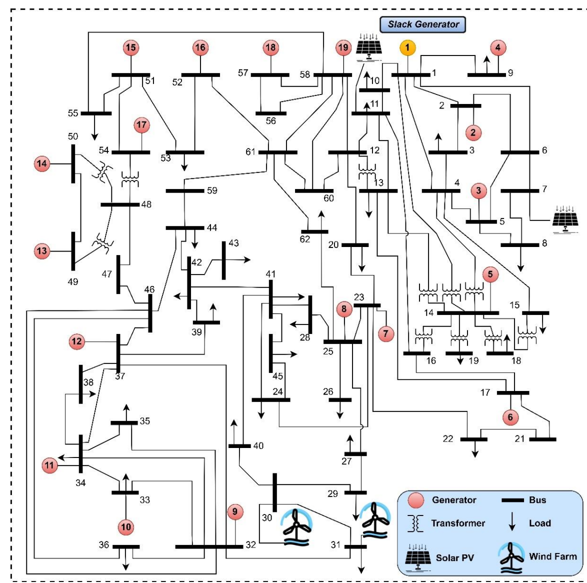

Fig. 6. Single line diagram of Modified 62 bus Indian system.

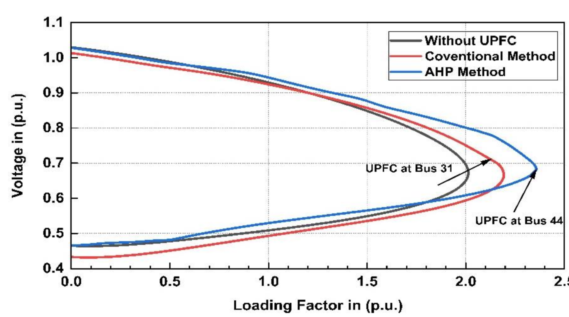

Fig. 7. PV Curve comparison for the Indian 62 Bus system.

Table 2. Consistency Ratio of AHP method.

Matrix size	1	2	3	4	5	6	7	8	9	10
Random Index (RI)	0	0	0.58	0.90	1.12	1.24	1.32	1.41	1.45	1.49

Table 3. Matrix for pairwise comparisons.

Objective function	**Stability margin**	**Voltage deviation**	**Real power loss**	**Weights (AHP)**
Stability Margin	1	7	9	0.777
Voltage Deviation	$\frac{1}{7}$	1	3	0.155
Real Power Loss	$\frac{1}{9}$	$\frac{1}{3}$	1	0.069

Table 4. Test system descriptions using RES.

Parameter	**Indian 62-Bus**
Quantity of buses	62
Quantity of lines	89
Quantity of load buses	32
Quantity of generators	19
Quantity of tap changers	11
Quantity of shunt capacitors	2
Quantity of regulating variables	32
Base-case real power load	2909 MW
Base-case reactive power load	1207 Mvar
Real power losses at base case	68.066 MW
Location of WFs	Bus 30 and 31
WF sizes	500 MW each
Location of SPV	Bus 7, 11
Rated capacities of SPV	50 MW each

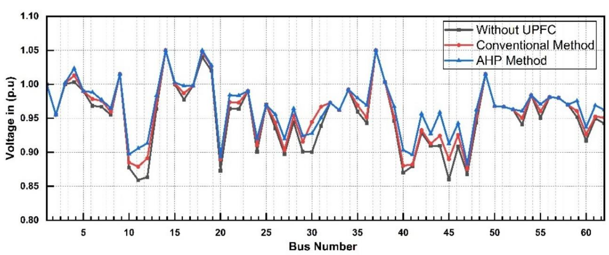

Fig. 8. Voltage magnitude comparison for the Indian Utility 62 Bus system.

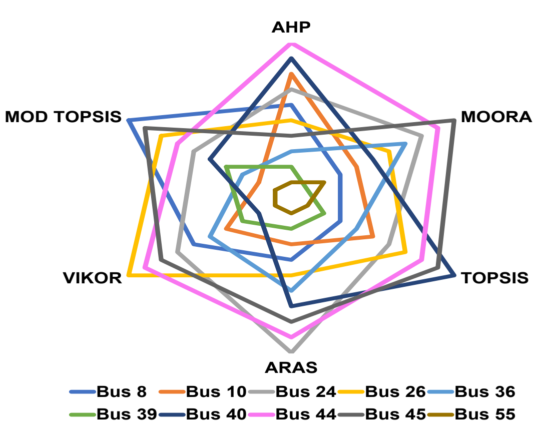

Fig. 9. Borda score comparison for the AHP, MOORA, TOPSIS, ARAS, VIKOR, Mod TOPSIS methods.

The functions f_1, f_2, and f_3 are defined above.

Table 5. Minimum values for the objective function in the Indian 62-bus system.

Bus No.	f_1	f_2	f_3	F
Bus^{03}	0.01687	0.01719	0.01678	0.01693
Bus^{08}	0.01677	0.01575	0.01694	0.01664
Bus^{09}	0.01687	0.01724	0.01678	0.01694
Bus^{10}	0.01662	0.01578	0.01751	0.01657
Bus^{11}	0.01682	0.01710	0.01682	0.01688
Bus^{13}	0.01687	0.01712	0.01676	0.01692
Bus^{15}	0.01686	0.01699	0.01681	0.01689
Bus^{18}	0.01687	0.01722	0.01679	0.01694
Bus^{19}	0.01687	0.01710	0.01678	0.01692
Bus^{20}	0.01681	0.01719	0.01687	0.01689
Bus^{22}	0.01692	0.01689	0.01691	0.01693
Bus^{24}	0.01675	0.01576	0.01696	0.01663
Bus^{26}	0.01653	0.01727	0.01738	0.01672
Bus^{27}	0.01679	0.01684	0.01691	0.01682
Bus^{28}	0.01687	0.01715	0.01678	0.01692
Bus^{29}	0.01687	0.01719	0.01678	0.01693
Bus^{31}	0.01687	0.01716	0.01677	0.01692
Bus^{33}	0.01687	0.01718	0.01677	0.01693
Bus^{34}	0.01687	0.01721	0.01677	0.01693
Bus^{35}	0.01676	0.01726	0.01703	0.01687
Bus^{36}	0.01667	0.01725	0.01679	0.01678
Bus^{38}	0.01686	0.01713	0.01683	0.01692
Bus^{39}	0.01668	0.01709	0.01706	0.01679
Bus^{40}	0.01661	0.01566	0.01783	0.01656
Bus^{41}	0.01688	0.01590	0.01787	0.01681
Bus^{42}	0.01702	0.01578	0.01751	0.01688
Bus^{43}	0.01687	0.01701	0.01652	0.01688
$\boldsymbol{Bus^{44}}$	**0.01665**	**0.01588**	**0.01656**	**0.01654**
Bus^{45}	0.01682	0.01629	0.01691	0.01676
Bus^{53}	0.01688	0.01641	0.01674	0.01681
Bus^{55}	0.01686	0.01640	0.01678	0.01680
Bus^{62}	0.01687	0.01668	0.01673	0.01685

$$F = \omega_1 f_1 + \omega_2 f_2 + \omega_3 f_3 \tag{27}$$

Subject to:

$$\omega_1 + \omega_2 + \omega_3 = 1 \tag{28}$$

$$0 < \omega_1, \omega_2, \omega_3 < 1 \tag{29}$$

Where $\omega_1, \omega_2, and \ \omega_3$ are the weighting factors for the load margin, voltage deviation, and active power loss objective functions, respectively.

The priorities are considered when choosing the multi-objective optimization weighting factors. Voltage stability has thus been

Table 6. Comparative analyses of stability margin and power losses before and after Placing UPFC.

Sl. No.	Method of Placement	UPFC Location	Stability Margin	P_{loss} (MW)	Q_{loss} (MVar)
1	Without UPFC	–	2.0132	68.066	35.007
2	Conventional Method	Bus 31 (Line 31–32)	2.1937	61.134	33.931
3	Proposed Method	Bus 44 (Line 44–46)	**2.3607**	56.006	**32.724**

Table 7. Comparison of the different MCDM rankings of Buses for UPFC location.

Rank	AHP	MOORA	TOPSIS	ARAS	VIKOR	ModTOPSIS
1	Bus^{44}	Bus^{45}	Bus^{40}	Bus^{24}	Bus^{26}	Bus^{08}
2	Bus^{40}	Bus^{44}	Bus^{45}	Bus^{44}	Bus^{44}	Bus^{45}
3	Bus^{10}	Bus^{24}	Bus^{44}	Bus^{45}	Bus^{45}	Bus^{26}
4	Bus^{24}	Bus^{36}	Bus^{26}	Bus^{40}	Bus^{24}	Bus^{44}
5	Bus^{08}	Bus^{26}	Bus^{24}	Bus^{36}	Bus^{08}	Bus^{24}
6	Bus^{26}	Bus^{40}	Bus^{10}	Bus^{26}	Bus^{36}	Bus^{40}
7	Bus^{45}	Bus^{10}	Bus^{36}	Bus^{08}	Bus^{10}	Bus^{39}
8	Bus^{36}	Bus^{08}	Bus^{08}	Bus^{10}	Bus^{39}	Bus^{36}
9	Bus^{39}	Bus^{55}	Bus^{39}	Bus^{39}	Bus^{40}	Bus^{10}
10	Bus^{55}	Bus^{39}	Bus^{55}	Bus^{55}	Bus^{55}	Bus^{55}

Table 8. Optimal location of UPFC for different contingencies.

Contingency number	Scenario	Stability margin (Before UPFC placement)	F	Optimal UPFC location	Stability margin (After UPFC placement)
SL1 (1–10)	Line failure across 1 and 10	1.9498	0.01684	Bus^{45} (Line 41–45)	2.2462
SL2 (51–55)	Line failure across 51 and 55	1.9578	0.01746	Bus^{44} (Line 44–46)	2.3607
SL3 (25–28)	Line failure across 25 and 28	1.8911	0.01672	Bus^{08} (Line 7–8)	2.1279
DL	Double line outage (1–10 and 51–55)	1.5997	0.01792	Bus^{44} (Line 44–46)	2.3607
Gen out	Generator outage at Bus^{25}	1.6993	0.01658	Bus^{40} (Line 27–30)	2.2946
–	Base case	2.0132	0.01654	Bus^{44} (Line 44–46)	2.3607

Table 9. Stability margins with solar and wind energy.

Solar Energy			Wind Energy		
Scenario	Without UPFC	With UPFC	Scenario	Without UPFC	With UPFC
Base case	2.0132	2.3607	Base case	2.0132	2.3607
50 MW at Bus^{07}	2.1236	2.4186	500 MW at Bus^{30}	2.0711	2.3873
50 MW at Bus^{11}	2.1251	2.4205	500 MW at Bus^{31}	2.0769	2.3908
50 MW at Bus^{07} and Bus^{11}	2.1333	2.4941	500 MW at Bus^{30} and Bus^{31}	2.1143	2.4212

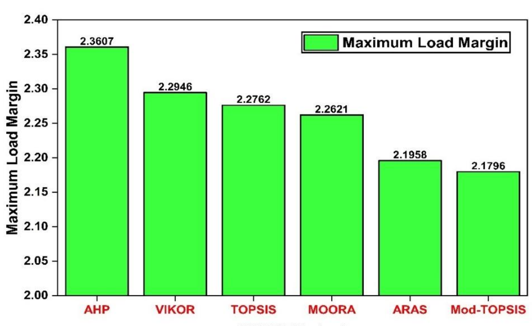

Fig. 10. Stability Margin Comparison of the different MCDM-based UPFC locations.

identified as the primary issue in the case study presented here.

Table 10. Stability margins with hybrid energy sources.

Hybrid Energy Scenario	Without UPFC	With UPFC
Base case	2.0132	2.3607
50 MW solar at Bus^{07} and 500 MW wind at Bus^{30}	2.1491	2.4346
50 MW solar at Bus^{11} and 500 MW wind at Bus^{31}	2.1610	2.4672
Two solar and two wind plants	2.2498	2.6842

The most important factor affecting voltage stability is load margin; active power losses and voltage variation have less of an effect. Using AHP, compare the criteria based on their relative

Table 11. Uncertainty analysis of voltage stability under different scenarios.

Scenario	Renewable Penetration (%)	Load Variation (%)	Stability Margin	P_{loss} (MW)	Q_{loss} (MVAr)	Probability of Occurrence (%)
Base case	30%	0%	2.0132	68.066	35.007	100%
High renewable, low load	50%	-10%	2.1456	64.12	33.865	15%
High renewable, high load	50%	10%	1.9235	72.32	38.012	20%
Low renewable, low load	20%	-10%	2.1809	62.55	32.785	10%
Low renewable, high load	20%	10%	1.8753	75.23	40.105	15%
Extreme contingency (line outage)	40%	0%	1.7650	78.412	42.576	5%
High renewable, peak load hours	50%	20%	1.7203	80.765	45.210	8%
Low renewable, peak load hours	20%	20%	1.6894	82.334	47.002	6%
Moderate renewable with grid congestion	35%	5%	1.9358	71.105	37.210	12%
Intermittent renewable with voltage fluctuation	45%	-5%	2.0501	67.543	34.784	18%

Table 12. Comparison of the suggested approach against existing methodologies.

Ref.	Case Studies / Validation	Impact of Renewable Sources	Multi-objective Function	Placement Strategy	Loadability Margin	Power Loss Reduction	Contingency Handling	Computational Complexity
[43]	Ethiopian Electric Power network	No explicit renewable integration	Active power loss and voltage deviation	Particle Swarm Optimization	Not emphasized	Effective reduction	Not considered	Moderate complexity
[44]	IEEE 14, 57, and 118 system	No renewable integration	Voltage deviation index and STATCOM cost	Mixed Integer Distributed Ant Colony Optimization	Not considered	Not considered	Not considered	High computational demand
[45]	IEEE 30, 57, and 118 system	No renewable integration	Total power loss and voltage deviations	Tunable Fuzzy PSO (APT-FPSO)	Not considered	Achieves power loss reduction	Contingency not emphasized	High due to hybrid approach
[46]	New England 39-bus system	Effective in wind-integrated systems	STATCOM cost and voltage deviation index	Mixed Integer Distributed Ant Colony Optimization	Not considered	Moderate loss reduction	Multiple uncertainties evaluated	High computational demand
[30]	Nigerian 330 kV system	No renewable integration	Loading parameter (λ)	Cuckoo Search algorithm	Strong focus on load margin improvement	Not considered	Not explicitly considered	High computational demand
[47]	IEEE 30 and 118 bus system	No renewable integration	Real power loss	African Buffalo Optimization	Not considered	Effective power loss reduction	Contingency scenarios addressed	High computation time
[48]	IEEE 30-bus system	No renewable integration	Active power loss and voltage deviation	Teaching Learning-Based Optimization	Not considered	Significant loss reduction	Not considered	Moderate complexity
Proposed method	Indian utility 62-bus system	Explicit focus on hybrid solar and wind integration	Load margin, power loss, and voltage deviation	Analytic Hierarchy Process (AHP)	Strong focus on load margin improvement	Significant loss reduction via multi-objective optimization	Explicit handling of contingency scenarios	Low (reduced complexity due to AHP structure)

importance to the overall objective. For example, voltage stability margin might be more important than voltage deviation, and power flow control might be prioritized over power loss reduction. Based on pairwise comparisons, calculate the weights for each criterion. This indicates how much each criterion contributes to the decision. Each alternative (potential location) is evaluated based on how well it satisfies each criterion. The matrix of pairwise comparisons indicating the significance of the criterion is given in Table 3.

5. Simulation Results and Discussions

The AHP method is implemented in a desktop system (DESKTOP-UIG4SB2) with an Intel (R) Core (TM) i5-8400 CPU operating at 2.80 GHz, 8.00 GB of RAM, and a 64-bit operating system is used to implement the proposed method to monitor VSM. A CPF program is simulated using PSAT [38] in the MATLAB 24 environment to find the maximum loading limit. The proposed approach is implemented on the Indian Utility 62 bus system covering various Tamil Nadu, India areas. This system has 19 generators, 11 transformers, and 89 transmission lines. The total system load demand is 2908 MW. The efficacy of the AHP method for the optimal location of UPFC is analyzed under various load conditions and different contingency scenarios. The wind farms (WF) locations are sourced from [39], and their validity is supported by a sensitivity-based analytical method. Additionally, the locations of solar photovoltaic (PV) plants are identified in [40]. Fig. 6 shows a renewable integrated 62-bus system layout for the Tamil Nadu state, India.

Table 4 describes integrating renewable sources in the Indian utility 62 bus systems. All wind farms consider a cut-in speed of 2.7 m/s, a cut-out speed of 25 m/s, and a nominal wind speed of 10 m/s. The solar irradiation is established at 1000 W/m^2 under conventional test circumstances.

The coefficients (weights) $\omega_1, \omega_2, and\ \omega_3$ are computed by the AHP method as 0.777, 0.155, and 0.069, respectively. The UPFC of 100 MVAr is considered to be installed at several locations, and the corresponding fitness values are given in Table 5.

Table 5 shows that although bus 40 offers the lowest power losses, the loading margin is unacceptable. In the same way, bus 43 has the finest voltage deviation and appropriate active power loss values but a relatively high loading margin. The compromised solution for the location of UPFC is identified as bus 44 leads, which has the highest fitness value. Therefore, this location is optimal.

CPF is carried out considering 200 MVAr UPFC at bus 44, and the PV curve is plotted as shown in Fig. 7. The loading factors with and without UPFC are also shown in the fig.7. Additionally, it compares the results with UPFC connected at bus 31 based on weak bus analysis [41] i.e., the conventional method to illustrate the effectiveness of the proposed method.

In a typical scenario, the system's loading margin is 2.01 after performing CPF. Accordingly, voltage collapse happens when the loading reaches 2.01 times the base load of the system. The loading margin reaches 2.19, which is nearly 8.96% improved for the UPFC linked at bus 31; however, for bus 44, the loading margin rises from 2.01 to 2.36, which is almost 17.26% enhanced for the system. From that, it is inferred that the AHP-based location of UPFC gives maximum load margin compared to Weak bus-based placement.

Fig. 8. demonstrates the comparison of voltage profiles in different scenarios. The AHP method-based UPFC placement shows improved results regarding the voltage profile in the case without UPFC and conventional method placement.

Table 6 compares real and reactive power losses for an Indian utility 62 Bus System before and after Placing UPFC. Compared to traditional methods, real and reactive power losses are much reduced in AHP-based placement.

The suggested approach is likewise contrasted to other MCDM methods, like TOPSIS, MOORA, ARAS, VIKOS, and Mod-TOPSIS, to give more insight into the proposed method. A comparison of the ranking of buses with different MCDM methods for UPFC locations is given in Table 7.

As evident from Table 7 results, most approaches can produce outcomes with comparable overall scores. The results show that bus 44 and bus 45 are typically the best locations for UPFC. The bottom ranks are likewise consistent; bus 55 is the worst location by almost all measures.

The AHP method is ranked equal to the BORDA solution [42], making it the most preferred approach in MCDM situations. Nevertheless, the rankings produced by alternative techniques cannot be disregarded or regarded as wholly incorrect due to the closeness of the numerical values discovered. The Borda value corresponding to the buses is shown on the radar chart in Fig. 9 for each approach.

The option with the highest overall score, as determined by the Borda count technique, is the best; bus 44 is the most appropriate location. Similarly, bus 8's placement is the worst, as is evident. The top-ranking buses from each MCDM method are chosen for UPFC placement, and the corresponding load margin after placing UPFC is shown in Fig. 10.

It is evident from Fig. 10, that the proposed AHP method gives the best load margin compared to all other MCDM methods. So, bus No 44 is an ideal location for UPFC to further analyze contingencies and a renewable integrated system. When the system's general performance is analyzed, the MCDM approaches are observed to provide comparable outcomes and converge to similar solutions. However, AHP predicts the solution better than any other MCDM technique.

To investigate the advantage of UPFC placement using the AHP method during contingency conditions, different types of contingencies are introduced to the network, and the performance is analyzed. Table 8 displays the results of the contingency analysis for each line loss involving a UPFC device in the Indian Utility 62 system.

The UPFC plays a pivotal role in ensuring Voltage stability in power systems combined with solar and wind energy by providing the flexibility and control necessary to confront the problems presented by the variable nature of renewable energy. With AHP, the UPFC can be located in areas that enable the integration of more renewable energy without compromising grid stability, thus supporting the transition to clean energy. The values of the stability margin, combined with the different kinds of renewable energy, are given in Tables 9 and 10.

A comprehensive uncertainty analysis assessed the impact of renewable energy integration and system loading variations on voltage stability. As shown in Table 11, the results highlight changes in voltage stability margin, active power losses, and reactive power losses under different operating scenarios, including normal conditions, high renewable energy penetration, increased load demand, and contingency events such as line outages.

The base case scenario, with 30% renewable penetration and no-load variation, establishes a reference with a voltage stability margin of 2.0132 p.u., active power loss of 68.066 MW, and reactive power loss of 35.007 MVar. When renewable penetration increases to 50% under low-load conditions (-10% variation), the system benefits from an improved voltage stability margin of 2.1456 p.u. and reduced power losses (64.120 MW active, 33.865 MVar reactive), demonstrating the positive impact of renewable integration when demand is low. However, under high-load conditions (+10% variation) with the same renewable penetration, the stability margin decreases to 1.9235 p.u. Power losses increase significantly (72.320 MW active, 38.012 MVar reactive), indicating higher grid stress.

Conversely, with lower renewable penetration (20%), the system exhibits better voltage stability in low-load conditions (2.1809 p.u.) but experiences increased power losses when the load rises, with the margin dropping to 1.8753 p.u. and power losses escalating (75.230 MW active, 40.105 MVar reactive). The most critical scenario, an extreme contingency (line outage) with 40% renewable penetration, results in the lowest voltage stability margin (1.7650 p.u.) and the highest power losses (78.412 MW active, 42.576 MVar reactive), emphasizing the vulnerability of the grid under stressed conditions. These results underscore the importance of the optimal placement of FACTS devices, enhanced contingency planning, and adaptive grid management strategies to maintain voltage stability and minimize power losses in modern renewable-integrated power systems.

A detailed comparison of the multi-objective function for voltage stability enhancement by AHP method-based UPFC placement in renewable-integrated power systems against existing literature is shown in Table 12.

This comparison underscores the advantages of the proposed method, particularly in renewable-integrated systems, where dynamic conditions and multiple objectives are critical. The AHP-based approach offers a well-rounded solution for modern power grids, handling complexity efficiently and ensuring stability under varied conditions.

6. CONCLUSION

This study introduces a practical multi-objective optimization framework to enhance voltage stability in renewable-integrated power systems, addressing real-world challenges such as renewable energy variability and system complexities. By incorporating objectives like maximizing loadability margin, minimizing power losses, and reducing voltage variance, the framework provides a systematic approach to optimizing UPFC placement. The AHP method ensures an effective balance between these competing operational priorities. The proposed method, validated on a solar- and wind-integrated Indian utility 62-bus system using MATLAB PSAT, confirms the effectiveness of the proposed approach. The results demonstrate a 17.24% improvement in voltage stability, as the stability margin increased from 2.0132 to 2.3607. Additionally, the proposed method achieved a 17.72% reduction in active power loss, decreasing from 68.066 MW to 56.006 MW, and a 6.53% reduction in reactive power loss, reducing it from 35.007 MVAr to 32.724 MVAr. These improvements highlight the framework's capability to enhance system reliability, minimize power losses, and ensure operational efficiency under diverse loading conditions.

This research provides a scalable and actionable solution for utilities and power system operators to mitigate voltage instability in renewable-rich environments. Future work will explore larger power networks, advanced optimization techniques, and real-time applications to further strengthen grid resilience and performance.

ACKNOWLEDGEMENT

The authors acknowledge the use of artificial intelligence tools (e.g., ChatGPT by OpenAI) for language editing and clarity improvement during the preparation of this manuscript. The authors are fully responsible for the scientific content, analysis, and conclusions.

REFERENCES

[1] J. Jacob, "A background history of the sustainable development goals," *Sustain. Dev.*, pp. 1–13, 2024.
[2] A. T. Hachemi *et al.*, "Modified reptile search algorithm for optimal integration of renewable energy sources in distribution networks," *Energy Sci. Eng.*, vol. 11, no. 12, pp. 4635–4665, 2023.
[3] S. Maihemuti, W. Wang, H. Wang, and J. Wu, "Voltage security operation region calculation based on improved particle swarm optimization and recursive least square hybrid algorithm," *J. Mod. Power Syst. Clean Energy*, vol. 9, no. 1, pp. 138–147, 2021.
[4] A. Alshareef, R. Shah, N. Mithulananthan, and S. Alzahrani, "A new global index for short term voltage stability assessment," *IEEE Access*, vol. 9, pp. 36114–36124, 2021.
[5] K. Anthony and V. Arunachalam, "Voltage stability monitoring and improvement in a renewable energy dominated deregulated power system: A review," *e-Prime Adv. Electr. Eng. Electron. Energy*, vol. 11, p. 100893, 2025.
[6] K. Anthony and V. Arunachalam, "Application of cascaded neural network for prediction of voltage stability margin in a solar and wind integrated power system," *Eng. Appl. Artif. Intell.*, vol. 138, p. 109368, 2024.
[7] V. Ajjarapu and B. Lee, "Bibliography on voltage stability," *IEEE Trans. Power Syst.*, vol. 13, no. 1, pp. 115–125, 1998.
[8] S. K. Gupta *et al.*, "Optimal sizing of distributed power flow controller based on jellyfish optimizer," *J. Oper. Autom. Power Eng.*, vol. 12, no. 1, pp. 69–76, 2024.
[9] A. N. Zubidi, B. Ismail, I. M. A. Al Hamrounni, N. H. A. Rahman, and M. H. H. M. Rozlan, "The impact of integrating multi-microgrid system with facts devices for voltage profile enhancement and real power loss reduction in power system: A review," *Pertanika J. Sci. Technol.*, vol. 31, no. 2, pp. 633–653, 2023.
[10] S. K. Gupta and S. K. Mallik, "Enhancement in voltage stability using FACTS devices under contingency conditions," *J. Oper. Autom. Power Eng.*, vol. 12, no. 4, pp. 365–378, 2024.
[11] S. Nascimento and M. M. Gouvêa, "Multi-objective adaptive evolutionary algorithm to enhance voltage stability in power systems," *Int. J. Control Autom. Syst.*, vol. 19, no. 7, pp. 2596–2610, 2021.
[12] N. Rani and T. Malakar, "A reactive power reserve constrained optimum reactive power dispatch using coronavirus herd immunity optimizer," *Electr. Power Compon. Syst.*, 2022.
[13] M. T. Khan *et al.*, "Optimal placement of multiple distributed generators using a novel voltage stability indicator employing arithmetic optimization algorithm," *Comput. Electr. Eng.*, vol. 110, p. 108853, 2023.
[14] A. Naganathan and V. Ranganathan, "Improving voltage stability of power system by optimal location of facts devices using bio-inspired algorithms," *Circuits Syst.*, vol. 7, no. 6, pp. 805–813, 2016.
[15] S. K. Dheebika and R. Kalaivani, "Optimal location of SVC, TCSC and UPFC devices for voltage stability improvement and reduction of power loss using genetic algorithm," in *Proc. IEEE Int. Conf. Green Comput., Commun. Electr. Eng. (ICGCCEE)*, pp. 1–6, 2014.
[16] K. Juneja, "A fuzzy-controlled differential evolution integrated static synchronous series compensator to enhance power system stability," *IETE J. Res.*, vol. 68, no. 6, pp. 4437–4452, 2022.
[17] X. Shen, H. Luo, W. Gao, Y. Feng, and N. Feng, "Evaluation of optimal upfc allocation for improving transmission capacity," *Glob. Energy Interconnect.*, vol. 3, no. 3, pp. 217–226, 2020.
[18] M. El-Azab, W. A. Omran, S. F. Mekhamer, and H. E. A. Talaat, "Allocation of facts devices using a probabilistic multi-objective approach incorporating various sources of uncertainty and dynamic line rating," *IEEE Access*, vol. 8, pp. 167647–167664, 2020.
[19] S. S. Padaiyatchi, "Hybrid DE/FFA algorithm applied for different optimal reactive power dispatch problems," *Aust. J. Electr. Electron. Eng.*, vol. 17, no. 3, pp. 203–210, 2020.
[20] B. Singh, V. Mukherjee, and P. Tiwari, "GA-based optimization for optimally placed and properly coordinated control of distributed generations and static var compensator in distribution networks," *Energy Rep.*, vol. 5, pp. 926–959, 2019.
[21] S. K. Mahmoudi, M. E. H. Golshan, and R. Zamani, "Coordinated voltage control scheme for transmission system considering objectives and constraints of network and control devices," *Electr. Power Syst. Res.*, vol. 192, p. 106908, 2021.
[22] S. K. Effatpanah *et al.*, "Comparative analysis of five widely-used multi-criteria decision-making methods to evaluate clean energy technologies: A case study," *Sustainability*, 2022.
[23] Y. Amrane and N. E. Y. Kouba, "A multiobjective optimal VAR dispatch using facts devices considering voltage stability and contingency analysis," in *Predictive Modelling for Energy Management and Power Systems Engineering*, pp. 1–26, Elsevier, 2021.
[24] A. Ishizaka and A. Labib, "Review of the main developments in the analytic hierarchy process," *Expert Syst. Appl.*, 2011.
[25] T. Chen, G. Liu, and S. Ahmed, "Exploring challenges in implementing sustainable energy solutions and green tourism for eco-industrial parks in china," *J. Renew. Sustain. Energy*, vol. 16, no. 6, 2024.
[26] M. S. Syed, C. V. Suresh, and S. Sivanagaraju, "Impact of renewable sources on electrical power system," *J. Oper. Autom. Power Eng.*, vol. 12, no. 3, pp. 261–268, 2024.
[27] M. T. Hoq, M. A. A. Murad, M. Rokonuzzaman, and N. Hossain, "Assessing impact of large scale integration of wind and solar PV power generation on small signal and transient stability," in *Proc. 4th Int. Conf. Electr. Eng. Inf. Commun. Technol. (iCEEiCT)*, pp. 483–488, 2018.
[28] F. Milano, L. Vanfretti, and J. C. Morataya, "An open source power system virtual laboratory: The PSAT case and experience," *IEEE Trans. Educ.*, vol. 51, no. 1, pp. 17–23, 2008.
[29] B. Vijay Kumar and V. Ramaiah, "Enhancement of dynamic stability by optimal location and capacity of UPFC: A hybrid approach," *Energy*, vol. 190, p. 116464, 2020.
[30] N. H. Ikeli, C. E. Ashigwuike, and I. I. Alabi, "Investigation of the impact of PSO, ABC, BFO and Cuckoo search optimization techniques on UPFC device for sustainable voltage stability margin improvement," *J. Electr. Syst. Inf. Technol.*, vol. 10, no. 1, p. 27, 2023.
[31] O. Herbadji, "Optimal power flow using firefly algorithm with consideration of facts devices "UPFC"," *Int. J. Electr. Eng. Inform.*, vol. 7, no. 1, pp. 12–28, 2015.

[32] H. H. Goh, B. C. Kok, H. T. Yeo, S. W. Lee, and A. A. Mohd Zin, "Combination of TOPSIS and AHP in load shedding scheme for large pulp mill electrical system," *Int. J. Electr. Power Energy Syst.*, vol. 47, pp. 198–204, 2013.

[33] T. Witkowski, P. Antczak, and A. Antczak, "Multi-objective decision making and search space for the evaluation of production process scheduling," *Bull. Pol. Acad. Sci., Tech. Sci.*, vol. 57, no. 3, pp. 195–208, 2009.

[34] A. Mazza, G. Chicco, and A. Russo, "Optimal multi-objective distribution system reconfiguration with multi criteria decision making-based solution ranking and enhanced genetic operators," *Int. J. Electr. Power Energy Syst.*, vol. 54, pp. 255–267, 2014.

[35] S. Liu, Q. Zhao, M. Wen, L. Deng, S. Dong, and C. Wang, "Assessing the impact of hydroelectric project construction on the ecological integrity of the Nuozhadu nature reserve, southwest China," *Stoch. Environ. Res. Risk Assess.*, 2013.

[36] T. L. Saaty, "A scaling method for priorities in hierarchical structures," *J. Math. Psychol.*, vol. 15, no. 3, pp. 234–281, 1977.

[37] A. Awasthi and S. S. Chauhan, "Using AHP and dempster–shafer theory for evaluating sustainable transport solutions," *Environ. Model. Softw.*, vol. 26, no. 6, pp. 787–796, 2011.

[38] F. Milano, L. Vanfretti, and J. C. Morataya, "An open source power system virtual laboratory: The PSAT case and experience," *IEEE Trans. Educ.*, vol. 51, no. 1, pp. 17–23, 2008.

[39] N. Rani and T. Malakar, "A reactive power reserve constrained optimum reactive power dispatch using coronavirus herd immunity optimizer," *Electr. Power Compon. Syst.*, 2022.

[40] O. A. Ajeigbe, J. L. Munda, and Y. Hamam, "Optimal allocation of renewable energy hybrid distributed generations for small-signal stability enhancement," *Energies*, vol. 12, no. 24, p. 4777, 2019.

[41] A. Raj and A. K. Chandel, "Enhancement of voltage profile/stability by optimal placement of UPFC," in *Proc. IEEE Int. Conf. Convergence Technol.*, pp. 1–6, 2022.

[42] F. Aydin and B. Gümüş, "Comparative analysis of multi-criteria decision making methods for the assessment of optimal SVC location," *Bull. Pol. Acad. Sci. Tech. Sci.*, p. 140555, 2022.

[43] T. T. Wondie and T. G. Tella, "Voltage stability assessments and their improvement using optimal placed static synchronous compensator (STATCOM)," *J. Electr. Comput. Eng.*, vol. 2022, 2022.

[44] B. H. Al-majali and A. F. Zobaa, "A novel optimal allocation of STATCOM to enhance voltage stability in power networks," *Ain Shams Eng. J.*, vol. 15, no. 5, p. 102658, 2024.

[45] M. Nasouri Gilvaei, H. Jafari, M. Jabbari Ghadi, and L. Li, "A novel hybrid optimization approach for reactive power dispatch problem considering voltage stability index," *Eng. Appl. Artif. Intell.*, vol. 96, p. 103963, 2020.

[46] J. Liu, Y. Xu, and J. Qiu, "Non-network solution coordinated voltage stability enhancement with STATCOM and UVLS for wind-penetrated power system," *IEEE Trans. Sustain. Energy*, vol. 11, no. 3, pp. 1559–1568, 2020.

[47] G. Saha, K. Chakraborty, and P. Das, "Enrichment of voltage stability in power system through novel generalized approximate reasoning based intelligent control with african buffalo optimization approach," *Soft Comput.*, vol. 27, no. 11, pp. 7473–7496, 2023.

[48] R. Verma and A. Rathore, "Optimal placement of facts device considering voltage stability and losses using teaching learning based optimization," *J. Inst. Eng. (India) Ser. B*, vol. 102, no. 4, pp. 771–776, 2021.